New Physics: Sae Mulli,
Vol. 69, No. 3, March 2019, pp. 234∼239
http://dx.doi.org/10.3938/NPSM.69.234

Magnetic Heat Effects of FeCoNi Nanoparticles Coated on Edge-Oxidized Graphene Sheets Under an Alternating Magnetic Field

Jinu KIM · Ki Hyeon KIM*
Department of Physics, Yeungnam University, Gyeongsan 38541, Korea

Taehoon KIM · Byungmun JUNG
Composites Research Division, Korea Institute of Materials Science, Changwon 51508, Korea

(Received 12 December 2018 : revised 8 January 2019 : accepted 9 January 2019)

To evaluate the self-heat behaviors of the FeCoNi magnetic nanoparticles decorated on edge-oxidized graphene (EOG) nanosheets, are deposited FeCoNi magnetic nanoparticles on EOG by using an electroless plate method. The mean diameter of the FeCoNi nanoparticles coated on EOG (FCNEOG) was approximately 45 nm. The saturation magnetization and coercivity of FCNEOG were 157 emu/g and 105 Oe, respectively. The heat elevations of the FCNEOG in silicon oil were measured at alternating magnetic fields of 75, 100, 125 Oe with frequencies of 155, 250 and 355 kHz, respectively, under an initial temperature of 25°C. The maximum temperatures elevation increased from 38°C to 46°C at 125 Oe and 355 kHz at the concentration of FCNS was varied from 5 mg/ml to 10 mg/ml. The temperatures elevation varied from 4.2°C (75 Oe and 355 kHz) to 21.5°C (125 Oe and 355 kHz) and the specific loss powers varied from 2.8 W/g to 11.1 W/g for FeCoNi on GO at a concentration of 7 mg/ml.

PACS numbers: 75.50.Bb, 75.90.+w, 81.05.ue, 81.15.Pq, 81.20.-n
Keywords: FeCoNi, Graphene oxide, Electroless plating, Hyperthermia

I. INTRODUCTION

Two-dimensional graphene oxide (GO) sheets are one of the expected materials for various applications in industry due to the high specific surface area, light weight, high thermal conductivity and strong adsorption [1–5]. The hybrid GO with various metallic and magnetic nanoparticles have potential for industries such as electronic device, gas sensors, energy storage, wastewater purification and electromagnetic (EM) shield and absorption [5–10]. In particular, the hybrid GO with magnetic nanoparticles have been actively studied for applications such as electromagnetic interference (EMI) material and hyperthermia *etc* [10,11].

The magnetic nanoparticles can be heated under the alternating magnetic field (AMF) due to the eddy current, hysteresis and magnetic loss. Eddy current loss is governed by a skin depth of the material, which is defined by the applied frequency, the electrical conductivity and permeability of the material. However, the eddy current loss in nanoscale particles can be neglected in the range of a few hundred kHz. In magnetic loss of the magnetic particles, the magnetization reversal plays a critical role for hysteresis loss and relaxation. The hysteresis loss determined by the internal area of the hysteresis loop with the applied alternating magnetic field. Especially, the superparamagnetic nanoparticles (SPMN) generate the heat by the relaxation loss of particles in AMF because of the nearly zero coecivity. Therefore, the heat dissipation of SPMN are governed by the Neel and Brown relaxation. Neel rotation governs the restructuring of electronic spin states to allow the magnetic moment to reorient irrespective of the orientation of the whole particle. When the particle itself rotates in the solution, Brown relaxation is the reorientation of the magnetic

*E-mail: kee1@ynu.ac.kr

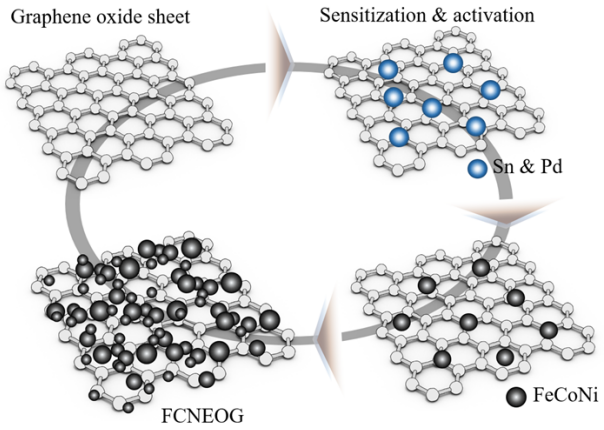

Fig. 1. (Color online) Synthesis process of FeCoNi coated on EOG by electroless plate.

particle itself in a fluid, resulting in friction of the particle with the fluid [12–14]. The self-heat of magnetic nanoparticles under AMF has been studied for the applications of treatments of malignant tumor cells and drug delivery, which is called hyperthermia. The malignant tumors can be destroyed by increasing the tumor temperature typically within the range 37∼ 45°C for hyperthermia or above 45°C for thermo-ablation [15]. These kinds of magnetic nanoparticles for hyperthermia treatments have some disadvantages of the moving particles in the body and the elimination time of particles from the body. Xiali Zhu et. al and Jagriti Gupta et. al. reported the hyperthermia effects and target delivery for the hybrid reduced graphene and iron oxide nanoparticles [15,16]. We employed the EOG instead of GO because the EOG has a more good electrical conductivity than GO due to the lack of oxygen in the plane. Therefore, we prepared the immovable hybrid EOG and magnetic particles in the body due to the extremely high specific surface area of EOG. And EOG would be helpful to dissipate the thermal energy of the magnetic particles due to the high thermal conductivity. To enhance the heat elevation, we synthesized the EOG combined with FeCoNi magnetic nanoparticles under AMF.

II. EXPERIMENTAL

The FeCoNi magnetic nanoparticles prepared by electroless plating method on the EOG as shown in Fig. 1. Prior to the electroless deposition process, the graphene

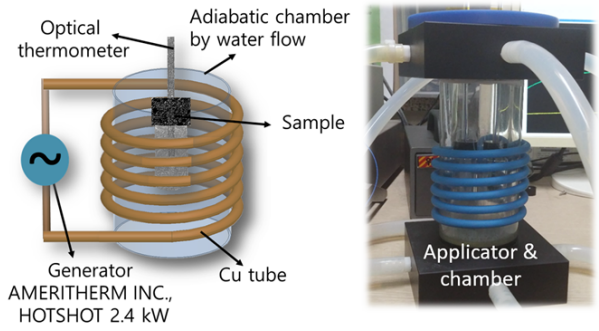

Fig. 2. (Color online) Schematic of induction heat system and the fabricated AMF applicator and chamber.

oxide sheets were sensitized and activated to prepare catalytic surface. Firstly, 0.2 g of water-soluble EOG (Mexplorer Inc.) was dispersed into 100 ml of aqueous solution containing 0.1 g of $SnCl_2$ and 1 ml of hydrochloric acid. Sensitization was performed by stirring the solution at 45°C for 30 min. The sensitized EOG was filtered and washed repeatedly, and subsequently dispersed into 100 ml of aqueous solution containing 0.2 g of $PdCl_2$ and 1 ml of hydrochloric acid. Activated EOG was obtained by the stirring the solution at 45°C for 30 min, filtering and washing. The activated EOG was dispersed in 3200 ml of plating solution containing iron sulfate heptahydrate ($FeSO_4{\cdot}7H_2O$, 0.06 M), cobalt sulfate heptahydrate ($CoSO_4{\cdot}7H_2O$, 0.01 M), nickel sulfate heptahydrate ($NiSO_4{\cdot}7H_2O$, 0.007 M), dimethylamine borane (DMAB, 0.26 M), sodium tartrate (0.2 M), sodium citrate (0.05 M), phosphorous acid (0.05 M), ammonium sulfate (0.2 M), and sodium hydroxide (14.4 g) at 75°C for 30 min. the hybrid EOG and FeCoNi particles were obtained by several washing and filtering process.

The morphologies and structures of FeCoNi magnetic nanoparticles on EOG were determined by using Transmission electron microscopy (TEM, HITACHI Ltd, H-7600), X-ray diffractometer (XRD, X'Pert PRO, PANalytical) with Cu Kα, $\lambda = 1.54059$ Å. The magnetic properties was measured by using Vibrating Sample Magnetometer (VSM, Lakeshore 7410). The induction heat temperature was measured by the heating system which is composed of RF power supply (AMERITHERM INC., HOTSHOT 2.4 kW) and 5.5 turns-helical shaped Cu coil with the 80 mm-height and 70 mm-inner diameter as an alternating current magnetic field applicator as shown in Fig. 2. The strength of AMF was measured by a magnetic field transducer (SENIS AG.). The temperature

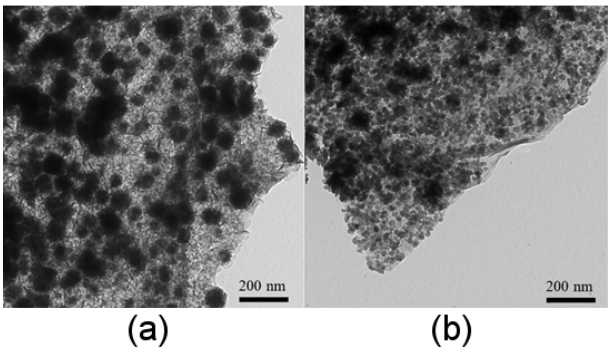

Fig. 3. TEM images of the hybrid EOG and FeCoNi magnetic nanoparticles.

was measured by using 4 channel thermometer (FISO, TMI4) and fiber optic probes (FISO, FOT-L-BA) with the resolution and accuracy of 0.1°C and ±1°C, respectively.

III. RESULTS AND DISCUSSION

The morphology of the FCNEOG was observed by using a TEM. The images showed the well deposited the FeCoNi magnetic nanoparticles on EOG plane, which the average particles size is approximately 45 nm as shown in Fig. 3. The FeCoNi magnetic nanoparticles on EOG exhibited the mixture of the agglomerated and single particles. The crystal structures of FCNEOG revealed that the peaks of 2 theta values are 45.2°, 65.8° and 83.5°, respectively. These peaks correspond to the (110), (200) and (211) reflection planes of Body Centered Cubic (BCC) FeCo phase (JCPDS card no. 48-1816 and 48-1817) as shown in Fig. 3(a). However, the EOG peaks were not detected which would be caused by the relatively lack of EOG contents in FCNEOG. The magnetic properties of FCNEOG showed good soft magnetic behaviors, which the saturation magnetization and coercivity of FCNEOG are obtained 157 emu/g and 105 Oe as shown in Fig. 3(b). These values are less than those of FeCo magnetic nanoparticles with 172 emu/g and 268 Oe [12].

The magnetic losses of heat generation can be expressed by the Specific Loss Power (SLP), which can be defined as the thermal dissipation per unit of mass of the

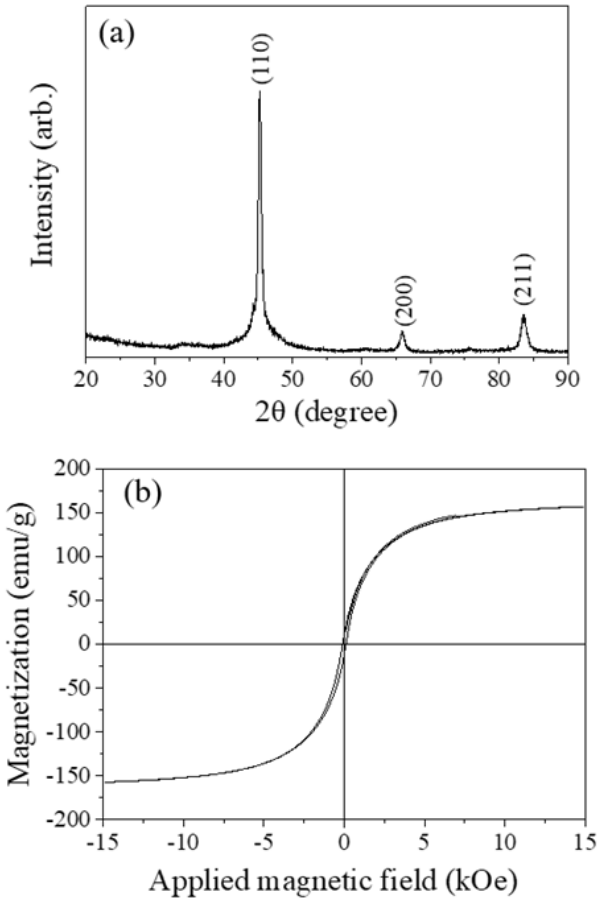

Fig. 4. X-ray diffraction pattern (a) and the magnetization curve (b) of hybrid EOG and FeCoNi magnetic nanoparticles.

magnetic material in the presence of an AMF. SLP is determined by [12,17]

$$\mathrm{SLP} = \mathrm{C_{sample}} \frac{\Delta T}{\Delta t} \frac{\mathrm{m_{sample}}}{\mathrm{m_{particles}}}. \quad (1)$$

Where $\mathrm{C_{sample}}$ is the specific heat capacity of the specimen with particles and solvent, $\mathrm{m_{sample}}$ and $\mathrm{m_{particle}}$ are the total mass of the specimen with the silicon oil and the mass of the particles without the silicon oil. In general, the specific heat capacity is the amount of heat energy required to raise the temperature of a substance per unit of mass. The specific heat is the heat capacity of the substance per gram of the substance. The $\Delta T/\Delta t$ is the initial slope of the time-temperature curve. The $\mathrm{C_{sample}}$ is expressed as follows.

$$\mathrm{C_{sample}} = \frac{(\mathrm{m_{particle}C_{magnetic}} + \mathrm{m_{solvent}C_{solvent}})}{\mathrm{m_{sample}}}. \quad (2)$$

Where $\mathrm{m_{solvent}}$ is the weight of silicon oil. The $\mathrm{m_{magnetic}}$ and $\mathrm{C_{solvent}}$ are the specific heat capacity, which are 0.45

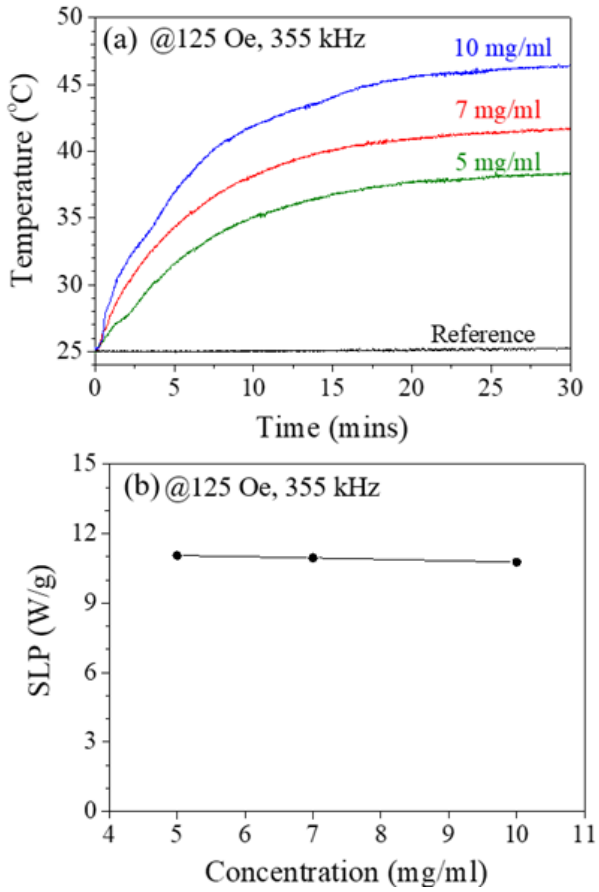

Fig. 5. (Color online) Heat elevation curves (a) and SLP (b) with the change of concentration with 5 mg/ml, 7 mg/ml and 10 mg/ml of FCNEOG under125 Oe at 355 kHz of AMF.

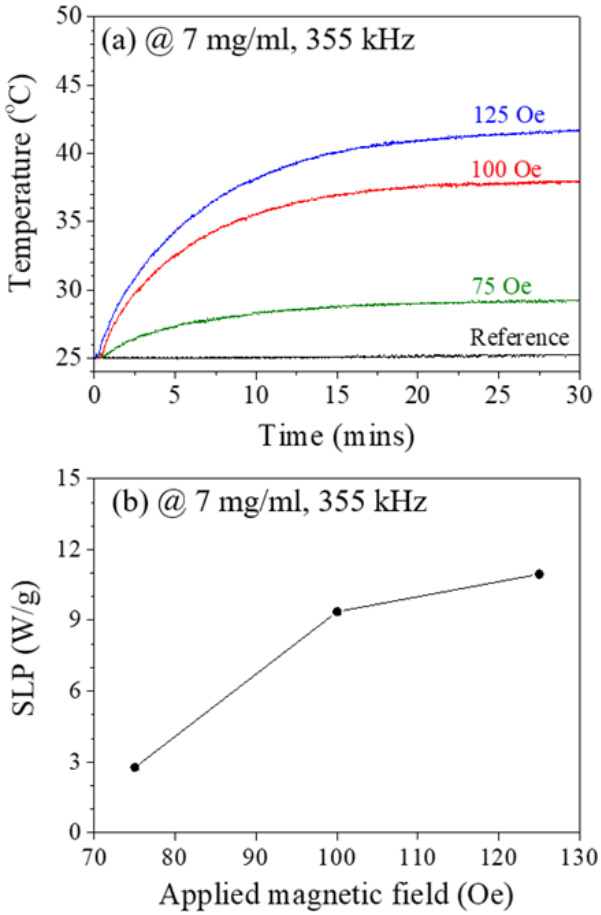

Fig. 6. (Color online) Heat elevation curves (a) and SLP (b) for the 7 mg/ml of FCNEOG with the change of AMF intensity of 75 Oe, 100 Oe and 125 Oe at 355 kHz, respectively.

J/gK for FeCoNi [18] and 1.6 J/gK for silicon oil [19]. The EOG mass can be neglected that the EOG mass ratios were relatively extreamly lower than that of FeCoNi particles.

The initial slope of the time-temperature curve is given by the phenomenological Box-Lucas equation as follows [20].

$$T(t) = T_{\text{initial}} + \Delta T_{\max}(1 - e^{(-t/\tau)}) \qquad (3)$$

Where T_{initial} and ΔT_{max} are the initial temperature of the specimen without AMF and the maximum saturation temperatures of the specimen when AMF applied, respectively.

To measure the heat elevation of the FCNEOG under AMF, the FCNEOG in silicon oil was placed in an isolated chamber with silicone oil without FCNEOG as a reference sample. In order to minimize the temperature variations of the inner part of chamber, the water is circulated along the chamber wall with 25°C. The temperature of the reference specimen was concurrently measured with FCNEOG for the reliability of the temperature variations under AMF.

The heating behaviors of FCNEOG evaluated with the change of FCNEOG concentration in silicon oil with 5, 7 and 10 mg/ml under AMF intensity of 125 Oe at 355 kHz as shown in Fig. 5. The temperatures elevated up to 38°C, 41°C and 46°C for 5 mg/ml, 7 mg/ml, and l0 mg/ml of FCNEOG, respectively, as shown in Fig. 5(a). The temperature of the silicone oil without FCNEOG kept at 25°C of initial temperature although the temperature of FCNEOG are elevated. The SLP values with the increment of FCNEOG exhibited the similar values of approximately 11 W/g as shown in Fig. 5(b). It implies that the experimental system is reliable for heating evaluation. In general, the SLP indicates the amount

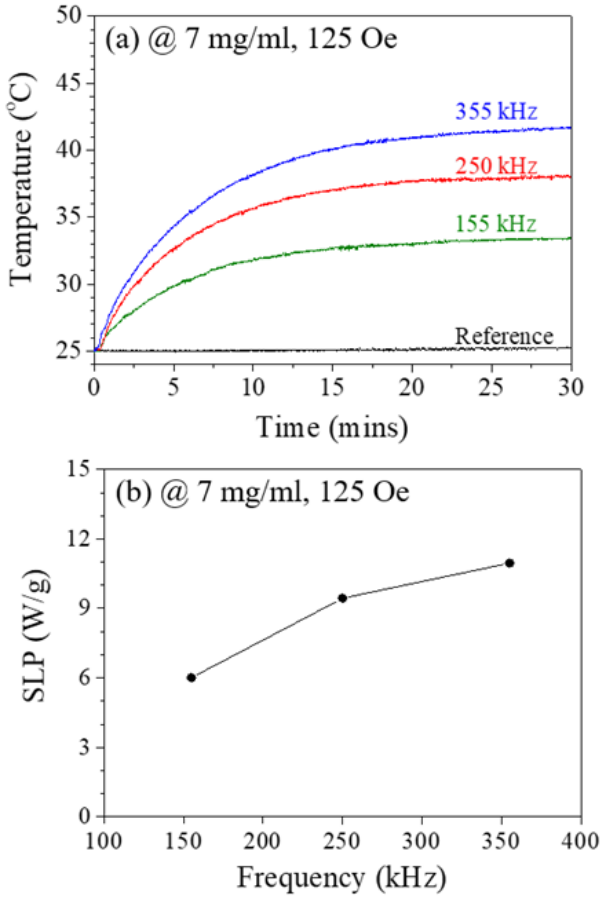

Fig. 7. (Color online) Heat elevation curves (a) and SLP (b) for the 7 mg/ml of FCNEOG with the change of AMF frequency of 155 kHz, 250 kHz and 355 kHz at 125 Oe, respectively.

of heat dissipations per unit mass. Therefore, the SLP values should be nearly consistent under same AMF conditions regardless of concentrations of specimens.

The maximum saturation temperatures for the 7 mg/ml of FCNEOG reached up to 29°C, 38°C and 41°C with the change of AMF intensity of 75 Oe, 100 Oe and 125 Oe at 355 kHz, respectively, as shown in Fig. 6(a). The SLP values were obtained 2.8, 9.4, and 11.1 W/g, which also increased with the change of AMF intensity, respectively, as shown in Fig. 6(b). Fig. 7(a) shows the maximum saturation temperatures of FCNEOG for 7 mg/ml with the increment of AMF frequency of 155 kHz, 250 kHz and 355 kHz at 125 Oe, which increased up to 33°C, 38°C and 41°C, respectively. The SLP values increased with the increase of AMF frequency which values are 6.0, 9.4, and 11.1 W/g, respectively, as shown in Fig. 7(b). The SLP of FCNEOG was less than that of the SLP of FeCo magnetic nanoparticles [12]. However, the FCNEOG would be immovable in the body due to the high specific surface area in comparison with that of FeCo nanoparticles. Overall the heating experiments showed a significant temperature increase of the FCNEOG concentration depending on the AMF intensity and frequency. The heat elevations of FCNEOG are in the range of 37 $\sim$ 45°C except the condition of 75 Oe at 355 kHz as mentioned in Introduction, which could be proper to the application of hyperthermia heat treatment.

IV. CONCLUSIONS

We synthesized and evaluated the hybrid graphene oxide with FeCoNi magnetic nanoparticles by electroless plating for self-heating effects under AMF. The temperatures and the SLP of FCNEOG increased with the increment of AMF intensity and frequency. The maximum temperature was 46°C for l0 mg/ml of FCNEOG under 125 Oe at 355 kHz. The maximum SLP was approximately 11 W/g at 125 Oe and 355 kHz. The FCNEOG can be one of good candidates for the applications of cancer treatments as an immovable heat source in the body due to the high specific surface area and thermal conductivity of graphene as well as the heat elevations.

ACKNOWLEDGEMENTS

This research was supported by Nano·Material Technology Development Program through the National Research Foundation of Korea (NRF) funded by the Ministry of Science, ICT and Future Planning (No. 2016M3 A7B4900267)

REFERENCES

[1] V. H. Luan, H. N. Tien, L. T. Hoa, N. T. M. Hien and E.-S. Oh *et al.*, J. Mater. Chem. A. **1**, 208 (2013).

[2] H. Zhao, X. Han, Z. Li, D. Liu and Y. Wang *et al.*, J. Colloid Interface Sci. **528**, 174 (2018).

[3] A. Li, C. Zhang and Y.-F Zhang, Polymers **9**, 437 (2017).
[4] S. Thangavel and G. Venugopal, Powder Technol. **257**, 141 (2014).
[5] T. A. Tabish, F. A. Memon, D. E. Gomez, D. W. Horsell and S. Zhang, Sci. Rep. **8**, 1817 (2018).
[6] T. Szabo, L. Nanai, D. Nesztor, B. Barna and O. Malina *et al.*, Adv. Mater. Sci. Eng. **1**, 1390651 (2018).
[7] T. Luqi, W. Danyang, J. Song, L. Ying and X. Qianyi *et al.*, J. Semicond. **37**, 041001 (2016).
[8] S. S. Varghese, S. Lonkar, K. K. Singh, S. Swaminathan and A. Abdala, Sens. Actuator B-Chem. **218**, 160 (2015).
[9] K. Chen, Q. Wang, Z. Niu and J. Chen, J. Energy Chem. **27**, 12 (2018).
[10] P. K. S Mural, S. P. Pawar, S. Jayanthi, G. Madras and A. K. Sood *et al.*, Appl. Mater. Interfaces **7**, 16266 (2015).
[11] S. Hatamie, M. M. Ahadian, M. A. Ghiass, A. I. Zad and R. Saber *et al.*, Colloid Surf. B-Biointerfaces **146**, 271 (2016).
[12] J. Kim, B. Nam and K. H. Kim, J. Kor. Phys. Soc. **69**, 344 (2016).
[13] S. A. Shah, D. B. Reeves, R. M. Ferguson, J. B. Weaver and K. M. Krishnan, Phys. Rev. B. **92**, 094438 (2015).
[14] S. A. Rovers, R. Hoogenboom, M. F. Kemmere and J. T. F. Keurentjes, J. Phys. Chem. C **112**, 15643 (2008).
[15] X. Zhu, H. Zhang, H. Huang, Y. Zhang and L. Hou *et al.*, Nanotech. **26**, 365103 (2015).
[16] J. Gupta, A. Prakash, M. K. Jaiswal, A. Agarrwal and D. Bahadur, J. Magn. Mag. Magn. **448**, 332 (2018).
[17] C. Guibert, V. Dupuis, V. Peyre and J. Fresnais, J. Phys. Chem. C **119**, 28148 (2015).
[18] Z. G. Wang, C. Dufour, E. Paumier and M. Toulemonde, J. Phys.: Condens. Matter **6**, 6733 (1994).
[19] B. Wang and S. Krause, Macromolecules **20**, 2201 (1987).
[20] R. R. Wildeboer, P. Southern and Q. A. Pankhurst, J. Phys. D: Appl. Phys. **47**, 495003 (2014).